Acta Crystallographica Section F
Structural Biology and Crystallization Communications
ISSN 1744-3091

X-ray crystallographic studies reveal that the incorporation of spacer groups in carbonic anhydrase inhibitors causes alternate binding modes

S. Zoë Fisher,[a] Lakshmanan Govindasamy,[a] Nicholas Boyle,[b]‡ Mavis Agbandje-McKenna,[a] David N. Silverman,[c] G. Michael Blackburn[b] and Robert McKenna[a]*

[a]Department of Biochemistry and Molecular Biology, College of Medicine, University of Florida, Gainesville, FL 32610, USA, [b]Department of Chemistry, University of Sheffield, Sheffield S3 7HF, England, and [c]Department of Pharmacology and Therapeutics, College of Medicine, University of Florida, Gainesville, FL 32610, USA

‡ Present address: Rady School of Management, Pepper Canyon Hall, 3rd Floor, 9500 Gilman Drive, MC 0093, La Jolla, CA 92093-0093, USA.

Correspondence e-mail: rmckenna@ufl.edu

Received 24 March 2006
Accepted 30 May 2006

PDB References: HCA II–BB3, 2eu3, r2eu3sf; HCA II–TDM, 2eu2, r2eu2sf.

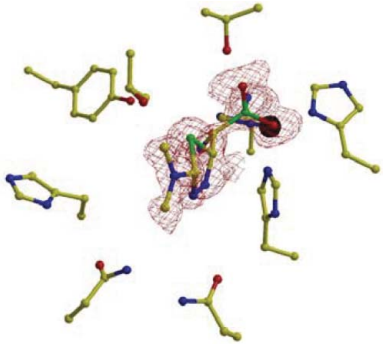

Human carbonic anhydrases (CAs) are well studied targets for the development of inhibitors for pharmaceutical applications. The crystal structure of human CA II has been determined in complex with two CA inhibitors (CAIs) containing conventional sulfonamide and thiadiazole moieties separated by a $-CF_2-$ or $-CHNH_2-$ spacer group. The structures presented here reveal that these spacer groups allow novel binding modes for the thiadiazole moiety compared with conventional CAIs.

1. Introduction

Carbonic anhydrases (CAs; EC 4.2.1.1) catalyze the interconversion of carbon dioxide and bicarbonate. The mammalian α-class of CAs (and the CA domains in more complex isoforms) are monomeric, with a molecular weight of approximately 30 kDa. At present, 14 human-expressed isoforms of CA (HCA I–XIV) are known, displaying widely varying tissue and subcellular distributions. They differ with regard to expression patterns, expression levels, kinetic properties and sensitivity to inhibitors (Tufts *et al.*, 2003; Duda & McKenna, 2004).

There is a wealth of information available on various CA inhibitors (CAIs) and their kinetic and structural characterization (for a general review, see Mansoor *et al.*, 2000; Supuran *et al.*, 2004). Briefly, various anions have historically been useful for studying the properties of the Zn active site of CA and it has been shown that most monovalent anions bind and inhibit CA activity to varying extents. These CAIs bind to the Zn^{2+} ion and interfere with the Zn-bound hydroxide coordination by either displacing or replacing the hydroxide, thus disrupting catalysis. A key residue in determining this displacement/replacement is Thr199, which is thought to act as a hydrogen-bond acceptor, stabilizing the Zn-bound hydroxide (Merz, 1990). Small anionic inhibitors (*e.g.* azide and cyanate) can bind directly to the zinc ion, thus substituting for the Zn-bound hydroxide. Inhibitors that bind in this way maintain hydrogen bonding with Thr199 and participate in the tetrahedral coordination of the Zn^{2+} ion.

The most frequently used pharmaceutical class of CAIs are aromatic and heterocyclic sulfonamides of the form $R-SO_2NH_2$ or $R-SO_2NH(OH)$. Several crystal complex structures of various sulfonamide inhibitors with various CAs have been determined and show similar interactions. The ionized NH group binds directly to the zinc and simultaneously donates a hydrogen bond to the hydroxyl group of Thr199 and an O atom of the sulfonamide group interacts with the amide backbone of Thr199 and in doing so displaces a second solvent molecule in the active site, termed the 'deep water' (Nair *et al.*, 1995). Fig. 1(*a*) shows the crystal structure of HCA II complexed with the clinically used inhibitor acetazolamide (Nair *et al.*, 1995).

CAIs are commonly prescribed to treat a major symptom of glaucoma: increased intraocular pressure. The inhibition of CA suppresses the secretion of sodium, bicarbonate and aqueous humor, thus lowering intraocular pressure (Maren, 1987). Clinically important drugs for the treatment of glaucoma include Diamox (acetazolamide) and Trusopt (dorzolamide) (Breinin & Gortz, 1954; Lippa *et al.*, 1992). Recently, aberrant expression of HCA IX has been shown to be associated with certain types of cancer, such as non-

small-cell lung cancer and renal-cell carcinoma. It is thought that the presence of CA in solid tumors may help cancerous cells to adapt to hypoxic conditions and could increase the invasiveness of these tumors (Wykoff *et al.*, 2000; Giatromanolaki *et al.*, 2001). Currently prescribed CAIs such as acetazolamide are not very soluble and it is believed that a drug with better water solubility would have improved bioavailability for the topical treatment of glaucoma and possibly cancer (Kim *et al.*, 2005). In the search for CAIs with improved water solubility and subsequent bioavailability, the Blackburn laboratory has recently synthesized a series of heterocyclic sulfonamides that have better water solubility than some of the conventional glaucoma treatments yet still bind HCA II with nanomolar affinity (Boyle *et al.*, 2005). These compounds have an additional spacer group, $-CF_2-$ or $-CHNH_2-$, between the classically employed sulfonamide moiety and the 1,3,4-thiadiazole ring (Figs. 1*b* and 1*c*, respectively).

We have determined the crystal structures of two of these compounds, namely 2-amino-1,3,4-thiadiazolyl-5-difluoromethanesulfonamide (BB3) and 2-dimethylamino-5-sulfonamido(aminomethyl)-1,3,4-thiadiazole (TDM), in complex with HCA II to 1.6 and 1.15 Å resolution, respectively. The structures show that the spacer allows the CAIs more conformational freedom and as a consequence alters the binding locations of the 1,3,4-thiadiazole ring within the

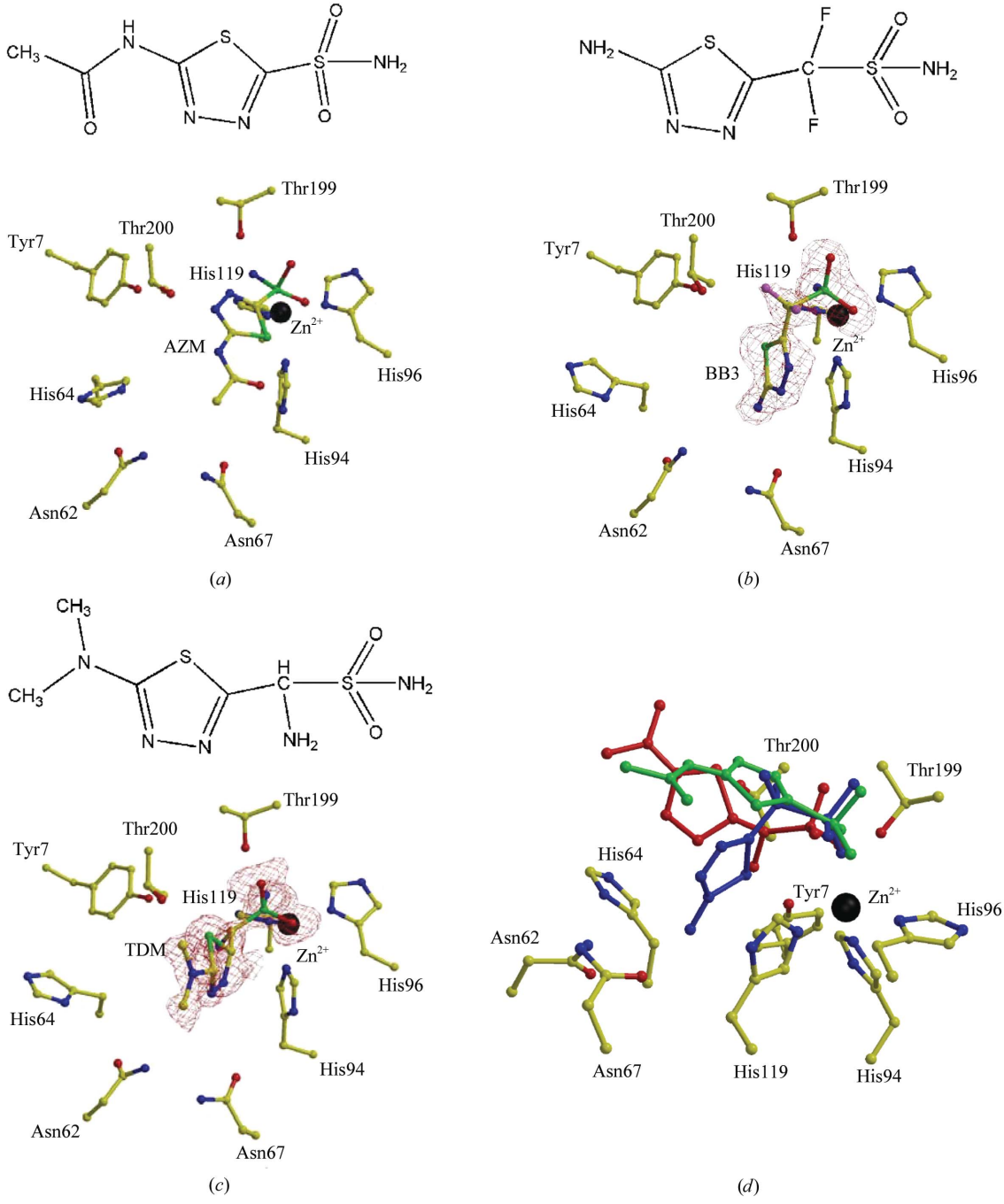

Figure 1
Structure of the active site of HCA II complexed with inhibitors. (*a*) Acetazolamide (AZM), (*b*) BB3, (*c*) TDM; (*d*) superimposition of all three: BB3, blue; TDM, red; AZM, green. The Zn atom is shown as a black sphere; side chains are as labeled. AZM coordinates were taken from PDB code 1yda (Nair *et al.*, 1995). The red $F_o - F_c$ electron-density map shown in (*a*) and (*b*) is contoured at 2σ and was calculated without the inhibitors present. Figures were generated and rendered with *BobScript* and *Raster3D*, respectively (Esnouf, 1999; Merritt & Bacon, 1997).

Table 1
Data-collection, refinement and final model statistics.

Values in parentheses are for the highest resolution shell.

	BB3	TDM
Data-collection statistics		
Space group	$P2_1$	$P2_1$
Unit-cell parameters (Å, °)	a = 42.3, b = 41.4, c = 72.1, β = 104.1	a = 42.5, b = 41.6, c = 72.7, β = 103.9
Resolution (Å)	20.0–1.60 (1.66–1.60)	20.0–1.15 (1.19–1.15)
Total No. of unique reflections	32031 (3154)	87379 (7896)
Completeness (%)	99.9 (100.0)	97.9 (89.3)
Redundancy	4.4 (4.3)	7.0 (4.1)
Overall $I/\sigma(I)$	17.1 (4.2)	26.4 (4.7)
R_{sym}†	0.066 (0.209)	0.099 (0.323)
Refinement statistics		
R_{cryst}‡	0.167	0.136
R_{free}§	0.212	0.166
R.m.s.d. for bond lengths (Å)	0.009	0.010
R.m.s.d. for angles (°)	1.490	1.315
Average B factors (Å^2)		
Main chain	16.7	14.1
Side chains	23.2	17.5
Solvent	31.8	32.9
Inhibitor	21.5	16.5
Ramachandran statistics (%)		
Most favored regions	87.9	88.8
Additionally allowed regions	12.1	11.2
No. of protein atoms	2039	2039
No. of solvent atoms	246	310
No. of inhibitor atoms	13	14

† $R_{sym} = \sum|I - \langle I\rangle|/\sum\langle I\rangle$. ‡ $R_{cryst} = \sum||F_o| - |F_c||/\sum|F_o|$. § R_{free} is calculated the same way as R_{cryst} for data omitted from refinement (5% of reflections for all data sets).

active site. These alternate binding modes are compared with other CAIs. The use of such spacers may offer a method of making CAIs that (i) are more soluble, (ii) have higher affinity and (ii) provide new binding modes of heterocyclic sulfonamides within the active-site cavity whose ring could be modified to target specific amino-acid differences between the various CA isoforms.

2. Experimental procedures

2.1. Expression and purification

Human CA II was expressed and affinity-purified as described elsewhere (Khalifah *et al.*, 1977). The protein purity of fractions was determined by silver-stained SDS–PAGE and fractions were pooled accordingly. Prior to crystallization, the protein was dialyzed against 50 m*M* Tris–HCl pH 7.8 and subsequently concentrated to ∼15 mg ml^{-1} with Amicon Ultra centrifugation filtration devices with a molecular-weight cutoff of 10 kDa. Final concentrations were determined by measuring the optical density at 280 nm and using a molar absorbance of 5.5×10^4 M^{-1} cm^{-1}.

2.2. Crystallization and diffraction data collection

Crystals of HCA II were grown using the hanging-drop method at room temperature (McPherson, 1982). The crystallization drops were prepared by mixing 5 µl protein (∼15 mg ml^{-1} in 50 m*M* Tris–HCl pH 7.8) with 5 µl precipitant solution (50 m*M* Tris–HCl pH 7.8, 2.6 *M* ammonium sulfate) and were equilibrated against 1000 µl precipitant solution. Useful crystals appeared within 5 d. The inhibitors BB3 and TDM were solubilized in water to a final concentration of 20 µ*M*. Pre-grown crystals of HCA II were then soaked in the presence of BB3 and TDM (at a final concentration of ∼1 µ*M*) for ∼24 h prior to data collection. The crystals were quick-dipped in cryoprotectant (30% glycerol in precipitant solution) before flash-freezing them at 100 K for X-ray data collection.

Diffraction data for the BB3-soaked HCA II crystals were collected at Brookhaven National Laboratory beamline X29 on a Quantum 315 CCD detector using a wavelength of 1.100 Å. The crystal-to-detector distance was set at 100 mm and oscillation images were collected in 1° steps for a total of 297 images.

Diffraction data for the TDM-soaked HCA II crystals were collected at Cornell High Energy Synchrotron Source beamline A1 on a Quantum 210 CCD detector using a wavelength of 0.978 Å. The crystal-to-detector distance was set at 100 mm and oscillation images were collected in 1° steps for a total of 410 images. Data-collection statistics are given in Table 1.

2.3. Structure determination and model refinement

X-ray diffraction data were indexed and scaled with *DENZO* and *SCALEPACK* from the *HKL* program package (Otwinowski & Minor, 1997). The structures were phased using molecular-replacement methods with the software package *Crystallography and NMR System* (*CNS*; Rossmann, 1990; Brünger *et al.*, 1998). The structure of HCA II (PDB code 1tbt) was used as the search model (Fisher *et al.*, 2005). After one cycle of rigid-body refinement, annealing by heating to 3000 K with gradual cooling, geometry-restrained position refinement and temperature-factor refinement, $F_o - F_c$ Fourier electron-density OMIT maps were generated (Figs. 1*b* and 1*c*). These maps clearly showed the position of the zinc and inhibitors, which were subsequently built into their respective electron density. The *PRODRG* server (http://davapc1.bioch.dundee.ac.uk/programs/prodrg/) was used to build coordinate and topology files for the inhibitors (Schüttelkopf & van Aalten, 2004). After initial refinement in *CNS*, R_{work} and R_{free} were 0.193 and 0.224 for the BB3 complex and 0.225 and 0.236 for the TDM complex, respectively.

Refinement of both models continued using *SHELXL*97 in the conjugate-gradient least-squares (CGLS) mode with *SHELXL* default restraints used for the protein geometry (Sheldrick & Schneider, 1997; Engh & Huber, 1991). After each round of ten cycles of CGLS refinement, Fourier electron-density maps ($F_o - F_c$ and $2F_o - F_c$) were calculated and minor manual model manipulations were performed using the molecular-graphics program *Coot* (Emsley & Cowtan, 2004). After several rounds of refinement, automated water divination was performed with *SHELX/WAT* using $F_o - F_c$ electron-density OMIT maps with a 4σ cutoff (Sheldrick & Schneider, 1997). For the TDM complex all non-H atoms were refined anisotropically, whereas only the Zn and S atoms of the BB3 structure were refined anisotropically, using the *SHELXL*97 default anisotropic displacement parameters (Sheldrick & Schneider, 1997). Manual model building included the modeling of alternate conformations for Ile22 and Lys39 for the TDM-complex structure and the addition/deletion of solvent molecules in both structures.

Refinement of the structures continued until convergence of R_{cryst} and R_{free} was reached. The final R_{cryst} and R_{free} were 0.167 and 0.212 for the BB3 complex (1.6 Å resolution) and 0.136 and 0.166 for the TDM complex (1.15 Å resolution), respectively. The model geometries were analyzed by *PROCHECK* and inhibitor–enzyme interactions were determined with *LIGPLOT* (Laskowski *et al.*, 1993; Wallace *et al.*, 1995). All data-refinement and final model statistics are given in Table 1.

3. Results and discussion

Here, we present the crystal structures of HCA II in complex with two novel CAIs termed BB3 and TDM. These compounds differ from

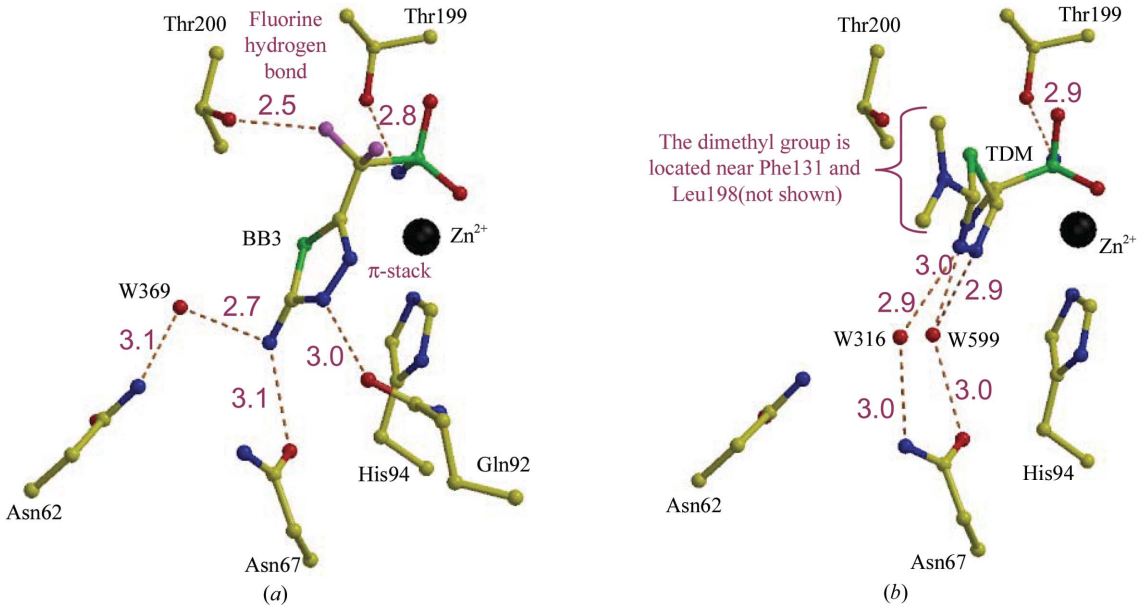

Figure 2
Interactions between HCA II and inhibitors. (*a*) BB3, (*b*) TDM. Hydrogen bonds are indicated by dashed red lines (distances given in Å), side chains are as labeled and the Zn atom is shown as a black sphere. Figures were generated and rendered with *BobScript* and *Raster3D*, respectively (Esnouf, 1999; Merritt & Bacon, 1997).

classical CAIs in that they contain a spacer group, $-CF_2-$ or $-CHNH_2-$, between the sulfonamide moiety and 1,3,4-thiadiazole ring for BB3 and TDM, respectively (Figs. 1*b* and 1*c*).

For both compounds the sulfonamide group maintains the same anchoring function as for other inhibitors in that the ionized NH group displaces the Zn-bound hydroxide and makes a hydrogen bond with Thr199 OG1. The N3 of the sulfonamide group is 2.8 and 2.9 Å from Thr199 OG1 in the BB3 and TDM structures, respectively. However, it was observed that the spacer and 1,3,4-thiadiazole ring of these compounds both adopt conformations in the active site of HCA II that differ from those of other CAIs (Fig. 1).

For BB3, the $-CF_2-$ spacer permits conformational rotational freedom between the sulfonamide and thiadiazole ring. Subsequently, the thiadiazole ring of BB3 folds back and adopts a planar conformation and forms a π-stacking interaction with His94 (Figs. 1*b* and 2*a*). This is a very different configuration to that observed for other CAIs, where the heterocyclic ring adopts a more extended conformation that leads out of the active site. Acetazolamide is given here as a contrasting example (Figs. 1*a* and 1*d*).

There are also several other observed interactions that mediate the binding of BB3 to HCA II. The most interesting is the inferred hydrogen bond (2.5 Å) between F2 of BB3 and Thr200 OG1 (Fig. 2*a*). In addition to the fluorine hydrogen bond, the N1 and NH_2 of the thiadiazole ring directly hydrogen bond with Gln92 OE1 and Asn67 OD1, respectively. An indirect hydrogen bond also exists between NH_2 of the thiadiazole ring and Asn62 ND2 through a solvent molecule W369 (Fig. 2*a*).

In order to assess whether the π-stacking interaction with His94 of the thiadiazole ring of BB3 is specific to the $-CF_2-$ spacer group, the structure of compound TDM, which has a $-CHNH_2-$ spacer group, was investigated (Fig. 1*c*). In this complex the thiadiazole ring did not exhibit the π-stacking interaction with His94, but instead the ring adopted a puckered conformation and a different position relative to both BB3 and acetazolamide (Fig. 1*d*). N2 and N3 of the thiadiazole ring hydrogen bond to solvent molecules W316 and W599, which are in turn hydrogen bonded to Asn67. Interestingly, unlike the fluorine hydrogen bond observed for compound BB3, the $-CHNH_2-$ spacer group does not appear to participate in any stabilization interactions (Fig. 2*b*).

The observed differences between the binding modes of BB3 and TDM may also in part arise from the dimethyl moiety of TDM, which is located in the hydrophobic region of the active site that contains amino acids Phe131 and Leu198 (Fig. 2*b*).

4. Conclusion

Carbonic anhydrases are a well studied target for the development of new inhibitors for pharmaceutical research and applications. CAIs are prescribed for the treatment of various diseases, such as glaucoma, and have potential for cancer therapy. Historically, CAIs have had poor solubility and bioavailability. We have determined the crystal structures of two novel water-soluble CAIs in complex with HCA II. These CAIs contain conventional sulfonamide and thiadiazole moieties with the addition of spacer groups. The spacers confer novel binding modes of thiadiazole within the active site that have not been observed in other sulfonamide-based CAIs. The ability to change the binding location of the heterocyclic ring of sulfonamide CAI may provide a useful tool in the development of CA isoform-specific inhibitors.

The authors thank the staff at Cornell High Energy Synchrotron Source and Brookhaven National Laboratory for their help and support during X-ray data collection. This work was supported by NIH grant GM25154, University of Florida College of Medicine start-up funds (RM) and a Studentship (to NAB) from Sheffield and Sheffield Hallam Universities.

References

Boyle, N. A., Chegwidden, W. R. & Blackburn, G. M. (2005). *Org. Biomol. Chem.* **3**, 222–224.
Breinin, G. M. & Gortz, H. (1954). *AMA Arch. Ophthalmol.* **52**, 333–348.
Brünger, A. T., Adams, P. D., Clore, G. M., DeLano, W. L., Gros, P., Grosse-Kunstleve, R. W., Jiang, J.-S., Kuszewski, J., Nilges, M., Pannu, N. S., Read,

R. J., Rice, L. M., Simonson, T. & Warren, G. L. (1998). *Acta Cryst.* D**54**, 905–921.
Duda, D. M. & McKenna, R. (2004). *Handbook of Metalloproteins*, edited by A. Messerschmidt, pp. 249–263. New York: John Wiley & Sons.
Emsley, P. & Cowtan, K. (2004). *Acta Cryst.* D**60**, 2126–2132.
Engh, R. A. & Huber, R. (1991). *Acta Cryst.* A**47**, 392–400.
Esnouf, R. M. (1999). *Acta Cryst.* D**55**, 938–940.
Fisher, S. Z., Hernandez Prada, J., Tu, C. K., Duda, D., Yoshioka, C., An, H., Govindasamy, L., Silverman, D. N. & McKenna, R. (2005). *Biochemistry*, **44**, 1097–1105.
Giatromanolaki, A., Koukourakis, M. I., Sivridis, E., Pastorek, J., Wykoff, C. C. & Gatter, K. C. (2001). *Cancer Res.* **61**, 7992–7998.
Khalifah, R. G., Strader, D. J., Bryant, S. H. & Gibson, S. M. (1977). *Biochemistry*, **16**, 2241–2247.
Kim, S., Rabbani, Z., Dewhirst, M., Vujaskovic, Z., Vollmer, R., Schreiber, E., Oosterwijk, E. & Kelley, M. (2005). *Lung Cancer*, **49**, 325–335.
Laskowski, R. A., MacArthur, M. W., Moss, D. S. & Thornton, J. M. (1993). *J. Appl. Cryst.* **26**, 283–291.
Lippa, E. A., Carlson, L. E., Ehinger, B., Eriksson, L. O., Finnstrom, K., Holmin, C., Nilsson, S. E., Nyman, K., Raitta, C. & Ringvold, A. (1992). *Arch. Ophthalmol.* **110**, 495–499.
McPherson, A. (1982). *Preparation and Analysis of Protein Crystals*. New York: John Wiley & Sons.
Mansoor, U. F., Zhang, Y.-R. & Blackburn, G. M. (2000). *Carbonic Anhydrases: New Horizons*, edited by W. R. Chegwidden, N. D. Carter & Y. H. Edwards, pp. 437–459. Basel, Switzerland: Birkhauser Verlag.
Maren, T. H. (1987). *Drug Dev. Res.* **10**, 255–276.
Merritt, E. A. & Bacon, D. J. (1997). *Methods Enzymol.* **277**, 505–524.
Merz, K. M. (1990). *J. Mol. Biol.* **214**, 799–802.
Nair, S. K., Krebs, J. F., Christianson, D. W. & Fierke, C. A. (1995). *Biochemistry*, **34**, 3981–3989.
Otwinowski, Z. & Minor, W. (1997). *Methods Enzymol.* **276**, 307–326.
Rossmann, M. G. (1990). *Acta Cryst.* A**46**, 73–82.
Schüttelkopf, A. W. & van Aalten, D. M. F. (2004). *Acta Cryst.* D**60**, 1355–1363.
Sheldrick, G. M. & Schneider, T. R. (1997). *Methods Enzymol.* **277**, 319–343.
Supuran, C. T., Scozzafava, A. & Conway, J. (2004). Editors. *Carbonic Anhydrase: Its Inhibitors and Activators*. Boca Raton, USA: CRC Press.
Tufts, B. L., Esbaugh, A. & Lund, S. G. (2003). *Comput. Biochem. Physiol. A*, **136**, 259–269.
Wallace, A. C., Laskowski, R. A. & Thornton, J. M. (1995). *Protein Eng.* **8**, 127–134.
Wykoff, C. C., Beasley, N. J., Watson, P. H., Turner, K. J., Pastorek, J. & Sibtain, A. (2000). *Cancer Res.* **60**, 7075–7083.